# The statistical shift of the chemical potential causing anomalous conductivity in hydrogenated microcrystalline silicon

R. W. Lof and R. E. I. Schropp[a)]
*Faculty of Science, Debye Institute for Nanomaterials Science, Nanophotonics–Physics of Devices, Utrecht University, P.O. Box 80.000, 3508 TA Utrecht, The Netherlands*

(Received 18 March 2010; accepted 19 July 2010; published online 24 September 2010)

The behavior of the electrical conductivity in hydrogenated microcrystalline silicon ($\mu$c-Si:H) that is frequently observed is explained by considering the statistical shift in the chemical potential as a function of the crystalline fraction ($X_c$), the dangling bond density ($N_{db}$), and the doping density ($N_d$). Our model shows that temperature dependent dc conductivity measurements above room temperature can be very well explained by (unintentional) micro doping of $\mu$c-Si:H. It is shown that the statistical shift in the chemical potential ($\mu$) is influenced mostly by the ratio between $N_d$ and $N_{db}$. It is concluded that the anomalous dependence of the apparent activation energy ($E_a$) and the apparent exponential prefactor ($\sigma_0$) on $X_c$ can be explained by behavior of $\mu$, that can be induced by a change in this ratio between $N_d$ and $N_{db}$. We used an effective medium approximation for the electron density of states (DOS) of $\mu$c-Si:H. The DOS is calculated as a weighted sum of the DOS of c-Si and the DOS of a-Si:H, parameterized by $X_c$, $N_{db}$, and $N_d$. The conductivity is deduced assuming a single dominant conduction path above the conduction edge of a-Si:H. © *2010 American Institute of Physics*. [doi:10.1063/1.3478741]

## I. INTRODUCTION

Hydrogenated microcrystalline silicon ($\mu$c-Si:H), nowadays also called nanocrystalline silicon (nc-Si:H), is an interesting material for thin film electronic devices, such as solar cells. The transport properties of this material are investigated extensively by different groups.[1–7] Several theoretical models have been proposed to describe its transport properties,[5,8,9] but some issues are still under debate. One of them is the anomalous behavior [above room temperature (RT)] of the activation energy $E_a$ and the conductivity prefactor $\sigma_0$ (as derived empirically from an Arrhenius plot of the electrical conductivity) as a function of the crystalline ratio $X_c$.[10] With increasing crystallinity, $E_a$ drops to values far below that of intrinsic c-Si and $\sigma_0$ can suddenly drop by several orders of magnitude.

$\mu$c-Si:H has a multiphase structure consisting of small grains of c-Si embedded in a matrix of a-Si. At fixed growth conditions the structure grows inhomogeneously in the growth direction. Depending on the type of substrate and the growth conditions, it starts off, as a pure amorphous incubation layer, subsequently forming nanocrystals randomly distributed over the surface. The crystalline phase expands as the film thickens, forming cones consisting of smaller domains. Eventually the layer grows thick enough for the cones to merge and form large grain aggregates, which seem to be separated by thin walls of amorphous, or disordered tissue.[2] Formation of mid gap states, in the form of silicon dangling bonds, is hard to control during growth and at increasingly high $X_c$, the probability of incorporating oxygen and other contaminants increases.[11,12] If extended voids are present, also after deposition the material can easily become contaminated with moisture or oxygen. Due to the complex growth mechanism and unstable nature of the material in air the characterization and modeling of materials with high $X_c$ with respect to conductivity is ambiguous.

At very low temperatures, conduction is dominated by variable range hopping between mid gap states[5] or by tunneling of carriers between neighboring conducting crystals.[13] However, our concern is the anomalous behavior of the $E_a$ and $\sigma_0$ as a function of $X_c$ in experiments above RT. In these experiments $E_a$ can drop rapidly to low values [below 0.2 eV (Refs. 7 and 13)] and $\sigma_0$ can drop at the same time by up to three orders of magnitude with increasing $X_c$.[10] This behavior has been found to coincide with the formation of large aggregates of small crystals and has been attributed to changes in the transport path.[10] However, it is also found that transport properties mainly depend on the position of the Fermi level $E_f$ and on defect density.[14] According to Goerlitzer *et al.*[6] contamination by impurities (especially oxygen) is responsible for gradual variations in the electronic properties.

In this paper we show that the anomalous behavior of the conductivity can be modeled if we assume that there is some amount of n-type doping present in most of these materials. In particular, the observed decrease in $E_a$ and $\sigma_0$ as function of $X_c$ are manifestations of the statistical shift in the chemical potential ($\mu$).

## II. THE MODEL

The conductivity for n-type semiconductor can be written as the product of the carrier density ($n$), the electron charge ($e$), and the effective electron mobility ($\mu_e$),

$$\sigma = ne\mu_e. \tag{1}$$

The carrier density is calculated by integrating the prod-

a)Electronic mail: r.e.i.schropp@uu.nl.

 

uct of the density of states (DOS) distribution and the Fermi–Dirac distribution over all energies above the conduction edge $E_c$,

$$n = \int_{E_c}^{\infty} N(E,N_d,N_{db},X_c)f(E,\mu,T)dE. \quad (2)$$

Here $N(E,N_d,N_{db},X_c)$ is the DOS distribution parameterized by the doping density $N_d$, the dangling bond density $N_{db}$, and $X_c$. For the DOS we will use an effective medium approximation (EMA). With $N_d$ we take into account all possible electron donors (acceptors are ignored). This term excludes the density of dangling bonds, which is given by $N_{db}$. In the simulation (and in reality) the donor states will be partly occupied by electrons in correspondence with the Fermi–Dirac distribution. For simplicity, all donor states are assumed to be at a single energy level.

The chemical potential $\mu$ (not to be confused with the electron mobility $\mu_e$) is determined by the fact that the total number of (bound, trapped, or free) electrons in the material is fixed by the DOS and the doping. Therefore

$$n_{tot} = \int_{-\infty}^{\infty} N(E,N_d,N_{db},X_c)f(E,\mu,T)dE. \quad (3)$$

It follows from Eq. (3) that the chemical potential is a function of T and N and, therefore, a function of T, $N_d$, $N_{db}$, and $X_c$.

The basic assumption for $\mu$c-Si:H is that the dependence of the conductivity (above RT) on crystallinity is mainly determined by the behavior of the overall chemical potential, and much less by spatial fluctuations or by variations in the mobility. In more detail we consider the following:

(1) Small crystallites have boundary regions, which accommodate strain between the amorphous matrix and the crystallites.[15] The same is true for domain boundaries between grains. These regions could be considered as a third phase. The DOS of this third phase will be ignored because its contribution to long range transport is relatively small compared to the other phases. A DOS based on a mix of two phases (a-Si and c-Si) captures the essentials necessary for our purpose.

(2) During deposition, contaminants can be built in into the layer but they can also diffuse into the layer afterwards if a continuous volume of interconnected voids exists (such as cracks). The concentration of oxygen in the layer can vary over several orders of magnitude.[6,16] This contamination, and consequently the doping effect, seriously complicates the analysis of transport properties. For further discussion the exact origin of the doping effect is not relevant and we do not assume a specific (spatial) location of donor states in our model.

(3) It is known for a-Si that the concentration of dangling bonds increases with the doping density,[27] but it is very likely that at larger values of $X_c$ the doping is relatively more active in the crystalline fraction where this dopant compensation mechanism is not in effect. In our calculation we did not include this effect and treat $N_d$ and $N_{db}$ as independent parameters.

(4) We ignore spatial dependencies and therefore percolation[4,17] will play no role in our calculation, making our model more generally applicable. Percolation models cannot be applied to all types of $\mu$c-Si:H.[18]

(5) Details in the mobility function can be assumed to play a minor role in the evaluation of the integral in Eq. (2) above RT. Due to the presence of a sharp mobility edge, the conduction path can be assumed to be above the conduction band edge in the a-Si fraction. The temperature dependence of the mobility is known to be very weak. Thus, a single, temperature independent, mobility ($\mu_e$) will be assumed for all carriers above this conduction band edge. Normally the temperature dependence of $\mu_e$ is found to behave weakly activated as 1/T at high enough temperature[19] but we are interested in the behavior near RT and the temperature dependence of $\mu_e$ is therefore taken as negligible compared to doping effects.

(6) The number of conduction electrons will be calculated from the averaged DOS (weighted over c-Si and a-Si) using the Fermi–Dirac distribution. This procedure requires that band bending along the conduction path and charging effects are negligible. According to Liu *et al.*[5] the band bending is approximately 0.01 eV. We calculated (at $1000/T=3\ K^{-1}$) the Debye length ($L_d$) of the electrons in the conduction band inside the crystallites and found that for $E_c^{c\text{-}Si}-\mu>0.26$ eV the Debye length is larger than the dimensions of the crystallites (<100 nm). Thus, we can ignore band bending in our model but it should be kept in mind that for very high crystallinity band bending may play a role.

(7) The temperature dependence of the band gap is taken into account as a correction factor on the energy scale of the DOS. The value that we use is derived from the temperature dependence of the band gap of c-Si: $dE/dT=4.73\times10^{-4}T/(T+636)$ eV $K^{-1}$.[20] The introduction of the temperature dependence affects $\sigma_0$ but has very little effect on $E_a$.

## III. BAND STRUCTURE

In order to perform the calculations [Eqs. (1) and (2)] we need to know the electronic band structure of the material. We derived the DOS as a weighted average over both components (c-Si and a-Si).

For the band structure of c-Si we use the standard parabolic bands.[21] We have

$$N_V(E) = \frac{1}{2\pi^2}\left(\frac{2m_V}{\hbar^2}\right)^{3/2}\sqrt{E_V-E},$$

$$N_C(E) = \frac{1}{2\pi^2}\left(\frac{2m_C}{\hbar^2}\right)^{3/2}\sqrt{E-E_C}, \quad (4)$$

$E_C-E_V=1.1$ eV
$m_C=0.386m_0$
$m_h=0.260m_0$

For the band structure of a-Si we use the standard model with parabolic bands, exponential tails and a double Gaussian for the dangling bonds. For the conduction band we have[22]

$$\begin{aligned} &N_{CB+CBT}(E) = N_{CB}(E) \ \text{ for } \ E \geq E_C^{tail}, \\ &N_{CB+CBT}(E) = N_{CBT}(E) \ \text{ for } \ E \leq E_C^{tail}, \\ &N_{CB}(E) = N_C^0 (E - E_C)^{1/2}, \\ &N_{CBT}(E) = N_C^{tail} \exp\left[ - \frac{(E_C^{tail} - E)}{E_{C0}^{tail}} \right]. \end{aligned} \tag{5}$$

For the valence band we take

$$\begin{aligned} &N_{VB+VBT}(E) = N_{VB}(E) \ \text{ for } \ E \geq E_V^{tail}, \\ &N_{VB+VBT}(E) = N_{VBT}(E) \ \text{ for } \ E \leq E_V^{tail}, \\ &N_{VB}(E) = N_V^0 (E_V - E)^{1/2}, \\ &N_{VBT}(E) = N_V^{tail} \exp\left[ - \frac{(E - E_V^{tail})}{E_{V0}^{tail}} \right]. \end{aligned} \tag{6}$$

And for the dangling bonds we have

$$\begin{aligned} &N_{DB^{+/0}}(E) = \frac{N_{DB}^{tot}}{\sigma_{db}\sqrt{2\pi}} \exp\left[ - \frac{(E - E_{DB}^{+/0})^2}{(2\sigma_{db}^2)} \right], \\ &N_{DB^{0/-}}(E) = \frac{N_{DB}^{tot}}{\sigma_{db}\sqrt{2\pi}} \exp\left[ - \frac{(E - E_{DB}^{0/-})^2}{(2\sigma_{db}^2)} \right], \\ &N_{DB^{0/-}}(E) = N_{DB^{+/0}}(E + U), \\ &E_{DB}^{0/-} = E_{DB}^{+/0} + U. \end{aligned} \tag{7}$$

It is assumed that the mobility edges are located at the connection points: $E_C^{mob} = E_C^{tail}$ and $E_V^{mob} = E_V^{tail}$. Furthermore

| | |
|---|---|
| $E_C^{mob} - E_V^{mob} = 1.7$ eV | $E_{V0}^{tail} = 0.050$ eV |
| $E_C^{tail} - E_C = 0.02$ eV | $E_{C0}^{tail} = 0.035$ eV |
| $N_C^0 = 2 \times 10^{21}$ cm$^{-3}$ eV$^{-1}$ | $N_{DB}^{tot} =$ var (cm$^{-3}$) |
| $N_V^0 = 2 \times 10^{21}$ cm$^{-3}$ eV$^{-1}$ | $E_{DB}^{+/0} = 0.85$ eV |
| $N_V^{tail} = 3 \times 10^{20}$ cm$^{-3}$ eV$^{-1}$ | $U = 0.2$ eV |
| $N_C^{tail} = 3 \times 10^{20}$ cm$^{-3}$ eV$^{-1}$ | $\sigma_{DB} = 0.2$ eV |

A value for the band alignment of the crystalline conduction band with the amorphous mobility edge has recently been measured by Kleider *et al.*[23] Using these data, the band alignment of the two phases $E_C^{mob}$(a-Si) $- E_C$(c-Si) $= 0.15$ eV. The total number of silicon atoms is taken as $5 \times 10^{22}$/cm$^3$.

The total DOS is given by the weighted sum of the DOS of both phases plus the DOS of the doping ($N_d$).

$$N_{\mu c}(E) = X_C N_{c\text{-}Si}(E) + (1 - X_C) N_{a\text{-}Si}(E) + N_d(E_d). \tag{8}$$

In Fig. 1 we present an example of a DOS of the mixed material with doping. From simulations we concluded that the energy distribution of the doping levels is relatively unimportant at RT. Therefore, we have taken a single energy for the doping levels ($E_d$) at 0.15 eV below the conduction band edge of c-Si (and 0.3 eV below the conduction edge of a-Si). We do not assume any dominant (spatial) location of the dopants, whether it is in the crystalline phase, the amorphous phase, or at the interface between the two phases and we assume that the doping levels are at the same energy throughout the material. The position of the doping level is taken from values published for oxygen in c-Si.[24]

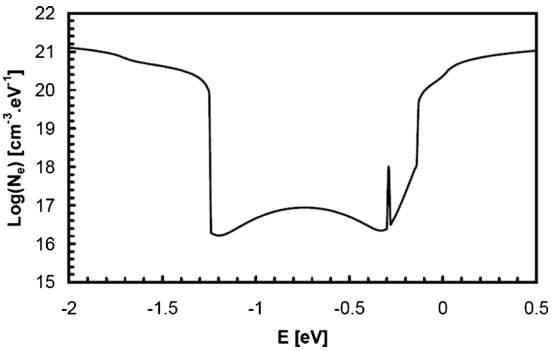


FIG. 1. The calculated DOS of $\mu$c-Si as a function of energy ($X_c = 0.5$, $T = 0$ K, $N_{db} = 5 \times 10^{16}$/cm$^3$ and $N_d = 10^{16}$/cm$^3$). The position of zero energy is taken at the mobility edge for electrons in a-Si. The sharp peak at 0.3 eV below the mobility edge are the dopant-related states.

Furthermore the conduction path is defined as the continuum of states throughout the material with energies above the conduction band edge in amorphous silicon. A value for $E_C$ can be derived from thin film transistor (TFT) measurements, from photoemission measurements,[22] or estimated from the lowest activation energies that have been measured above RT. In accordance with Ref. 22, we will assume $E_C$ to be 0.15 eV above the conduction band of c-Si.

## IV. RESULTS

In Fig. 2(a) we present the difference between the conduction band edge and the chemical potential ($\mu$). At low temperature $\mu$ is fixed at the Fermi level. The Fermi level is positioned in the upper half of the band gap. At higher temperatures (right from the dashed line) $\mu$ is shifting away from the conduction band toward the middle of the band gap.

Temperature dependent conductivity measurements are frequently analyzed in terms of a thermally activated single barrier conductivity relation:

$$\sigma = \sigma_0 e^{-E_a/kT}. \tag{9}$$

$E_a$ is called the apparent activation energy and $\sigma_0$ the apparent prefactor. Experimentally, $E_a$ is taken from the derivative in the $\ln[\sigma(1/T)]$-curve, also called Arrhenius plot, which often results in a temperature dependent $E_a$. We derived $E_a$ and $\sigma_0$ following this procedure. As an example of our calculations, we present the results for $E_c - \mu$, $E_a$, and $\sigma_0$ as a function of T in Figs. 2(a)–2(c). We have to keep in mind that below 300 K hopping will dominate and above about 400 K structural changes (such as H diffusion) may alter the material. Both effects are not accounted for in the model. The calculated results are therefore only applicable to experiments in a relatively small region above RT.

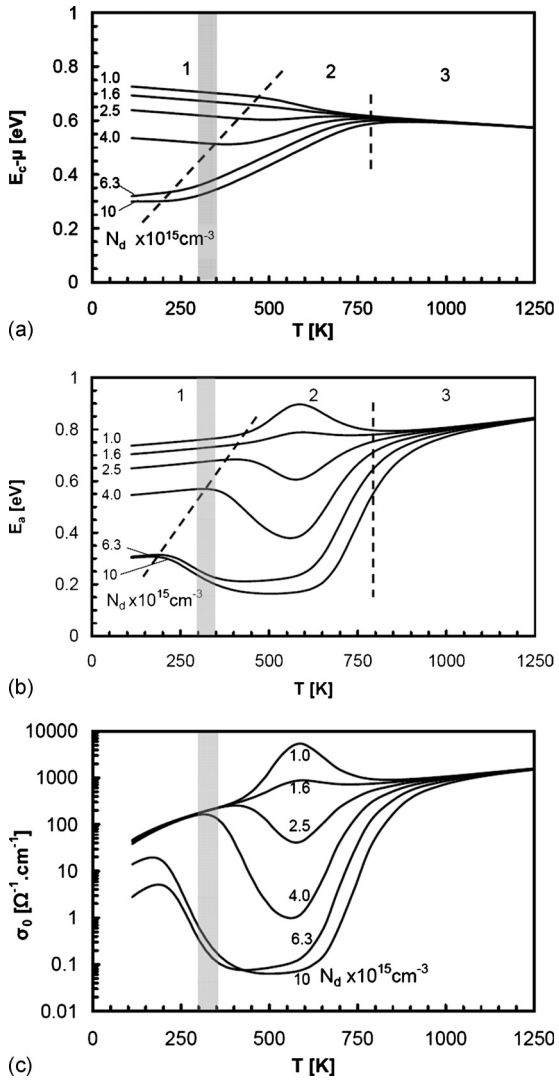


FIG. 2. (a) $E_c-\mu$ ($\mu$ is the chemical potential) as a function of T for different doping densities ($N_d$). The dotted lines indicate the boundaries between different regimes (1, 2, and 3). The gray band indicates the zone where so called RT values are experimentally determined. $N_{db}=10^{16}$ cm$^{-3}$, $X_c=0.5$. (b) $E_a$ as a function of T for different doping densities ($N_d$). $N_{db}=10^{16}$ cm$^{-3}$, $X_c=0.5$. (c) $\sigma_0$ as a function of T for different doping densities ($N_d$). $N_{db}=10^{16}$ cm$^{-3}$, $X_c=0.5$.

Comparing Figs. 2(a) and 2(b) we can distinguish three regimes: regime 3 starts far above any temperature that can give reliable results experimentally because of the unstable nature of $\mu$c-Si:H and a-Si:H at elevated temperatures but it shows that high-temperature conduction would be dominated by interband transitions, as expected. In the following, we will limit our discussion to regimes 1 and 2.

In regime 1, $E_a$ is nearly equal to $E_c-\mu$. But $E_c-\mu$ decreases with temperature due to the shrinkage of the band gap while $E_a$ increases due to the fact that the conduction band is a continuum (the average energy of the conduction electrons increases with temperature). Regime 1 is also characterized by the large differences of the Fermi level (at T=0) for different doping levels. For low doping densities ($N_d=10^{15}$ cm$^{-3}$) the Fermi level is only slightly above mid gap. At higher doping densities ($N_d=10^{16}$ cm$^{-3}$) the position of the Fermi level is located close to the doping level (0.3 eV below $E_c$).

In regime 2, $E_C-\mu$ starts to increase linearly with T, while $E_a$ is lowered (except for the top curves for low doping levels). This regime is characterized by the statistical shift in the chemical potential. Above a certain temperature the chemical potential starts to shift toward the mid gap position. During this shift the activation energy that would be measured is considerably lower than expected, which can be explained as follows. Let us assume that for $\mu$ a downward shift proportional to $T-T_s$ takes place, where $T_s$ is a threshold temperature. The conductivity can then be expressed as:

$$\sigma(T>T_s)=\sigma_M \exp\left[\frac{-(E_c-\mu)}{kT}\right]$$
$$=\sigma_M \exp\left[\frac{-E_c+E_f-\gamma_f k(T-T_s)}{kT}\right]$$
$$\equiv \sigma_0 \exp\left[\frac{-E_a}{kT}\right], \quad (10)$$

where $\gamma_f$ is a dimensionless parameter and $\sigma_M$ is the metallic conductivity limit.[25] In Eq. (10) we did not include the temperature dependence of $E_c$ explicitly for the sake of simplicity.

Normally $T_s$ is not taken into account[26,27] in the expression for $\sigma$ but this is not correct. Only when the shift in $\mu$ is caused by an asymmetry in the very near vicinity ($<kT$) of the Fermi level, $T_s$ is close to zero and can be left out of the equation. Since we are concerned about the statistical shift caused by the proximity of the conduction band (at a distance at least several kT above $\mu$) $T_s$ is in the order of RT and cannot be ignored. $T_s$ is identified with the dashed lines that indicate the border between regimes 1 and 2 in Figs. 2(a) and 2(b). Note that $T_s$ is almost proportional to $E_C-\mu$.

It follows from Eq. (10) that for $T>T_s$:

$$E_a=E_c-E_f-\gamma_f kT_s,$$
$$\sigma_0=\sigma_M e^{-\gamma_f}. \quad (11)$$

It can be concluded that, above the transition temperature $T_s$, $E_a$, and $\sigma_0$ are reduced by $\gamma_f kT_s$ and by a factor $\exp(-\gamma_f)$, respectively, due to the statistical shift. This is qualitatively consistent with the outcome of the simulation [Figs. 2(a) and 2(b)]. For instance, a value for $\gamma_f$ of 6.9 can be derived from a decrease in $\sigma_0$ by a factor 1000. Together with a $T_s$ of 250 K this leads to a reduction in $E_a$ by 0.15 eV at T slightly above RT.

Activation energies are commonly measured slightly above RT. These are found in the gray band in Figs. 2(a) and 2(b). They are located in regime 1 or regime 2 depending on crystallinity, defect density and amount of doping. This boundary between the two regimes can be crossed by a change in one of the parameters on which $\mu$ depends, T, $N_d$, $N_{db}$, and $X_c$. In the next paragraphs we will investigate how this boundary depends on $N_d$, $N_{db}$, and $X_c$.

We calculated (at $1000/T=3$ K$^{-1}$) the chemical potential ($\mu$) and the number of electrons in the conduction path, as a function of $X_c$, $N_d$, and $N_{db}$. From this we calculated $E_a$ and $\sigma_0$. In Figs. 3 and 4(a) we show three-dimensional (3D) plots of $E_a$ and $\sigma_0$ as a function of $N_d$ and $N_{db}$ at $X_c=0.5$. In

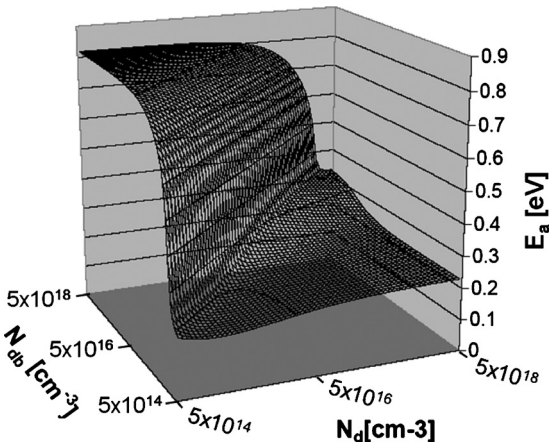


FIG. 3. Apparent $E_a$ as a function of $N_d$ and $N_{db}$ (Xc=0.5; T=333 K) in a 3D view.

Fig. 4(b) we present a contour map representation of the data presented in Fig. 4(a). Successive contours are one order of magnitude apart.

Both $E_a$ and $\sigma_0$ undergo a large change when raising $N_d$ or decreasing $N_{db}$. It is seen in Fig. 4(a) that for $N_d/N_{db} < 0.5$ the prefactor ($\sigma_0$) is nearly constant: $\sigma_0 \approx 200\ \Omega^{-1}\ \mathrm{cm}^{-1}$. At about $N_d/N_{db} \approx 0.5$ there is an abrupt large gradient in the $\sigma_0$-function perpendicular to this line.

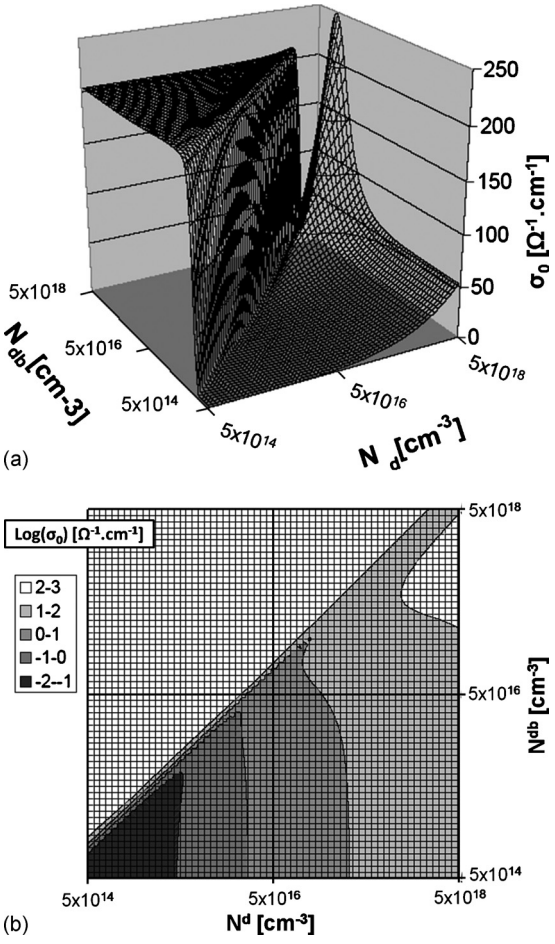


FIG. 4. (a) Apparent $\sigma_0$ as a function of $N_d$ and $N_{db}$ ($X_c$=0.5; T=333 K) in 3D view. (b) Contour map of Fig. 4(a) with logarithmic scale for the contours. Successive contours are one order of magnitude apart.

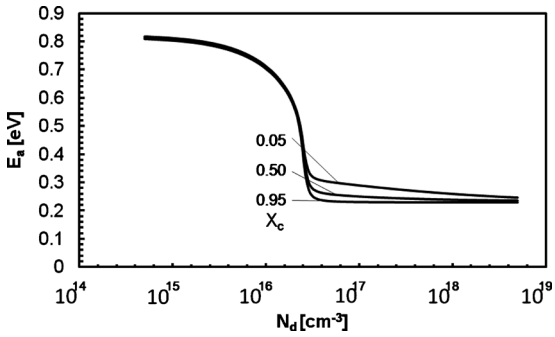


FIG. 5. Apparent $E_a$ as a function of $N_d$ for different $X_c$ (T=333 K; $N_{db} = 5 \times 10^{16}\ \mathrm{cm}^{-3}$).

For $N_d/N_{db} > 0.5$ the values of $\sigma_0$ are several orders of magnitude lower but in this regime $\sigma_0$ increases nearly linearly with $N_d$. For large dopant and large dangling bond densities $\sigma_0$ can again increase to values higher than 200 $\Omega^{-1}\ \mathrm{cm}^{-1}$. The region $N_d/N_{db} > 0.5$ is identified as regime 1 and the region $N_d/N_{db} < 0.5$ as regime 2 (the regimes are described in Sec. III). The activation energy changes from about 0.8 eV to a value between 0.2 and 0.3 eV when going from regime 1 to regime 2, while $\sigma_0$ can change several orders of magnitude when $N_d/N_{db}$ changes only 30%.

Next, we will focus on the influence of $X_c$ on $E_a$ and $\sigma_0$. Assuming no interdependence of parameters (such as an increased dopant concentration at an increased $X_c$), the influence of $X_c$ on $E_a$ is relatively small (see Fig. 5). Only after $E_a$ has dropped to lower values, the higher $X_c$ values show a lower $E_a$. The difference never exceeds 0.1 eV. In Fig. 6 the dependence of $\sigma_0$ on $X_c$ is shown for fixed $N_{db}$ and variable $N_d$. From the graph it is clear that the critical value for $N_d$ does not depend on $X_c$. Below the critical value (in regime 1) $X_c$ has no influence on $\sigma_0$. Only above the critical value (regime 2) there is a significant influence of $X_c$ on $\sigma_0$. The higher the crystallinity the larger the drop in $\sigma_0$, which is in agreement with experimental results. Ram *et al.*[28] records a drop in $\sigma_0$ of four orders of magnitude at a crystalline ratio of close to one, while Kočka *et al.*[10] observe a drop of three orders of magnitude at a crystallinity of 0.9.

The position of the transition stays in place when $X_c$ changes (we checked this also for a fixed $N_d$ and a variable $N_{db}$, with the same result). Therefore it can be concluded that the position of the transition is determined only by the ratio $N_d/N_{db} \approx 2$ found earlier. Since experiments show a sharp

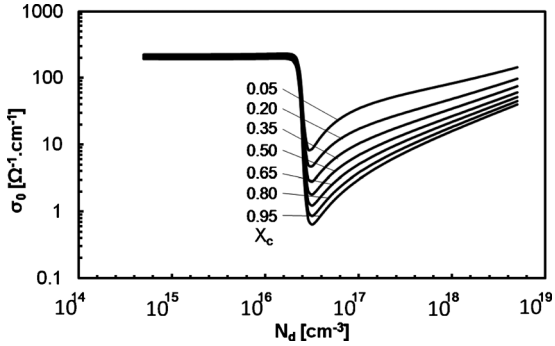


FIG. 6. Apparent $\sigma_0$ as a function of $N_d$ for different $X_c$ (T=333 K; $N_{db} = 5 \times 10^{16}\ \mathrm{cm}^{-3}$)

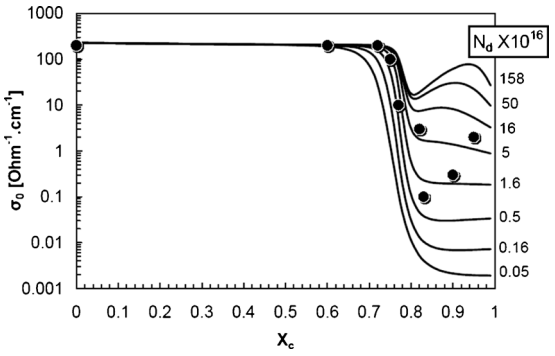


FIG. 7. Apparent $\sigma_0$ as function of $X_c$ for different dangling bond densities $N_{db}$ The ratio $(1-X_c)N_d/N_{db}$ is kept constant: $(1-X_c)$. $N_d/N_{db}=1/9$. Data is taken from Kočka *et al.* (Ref. 2).

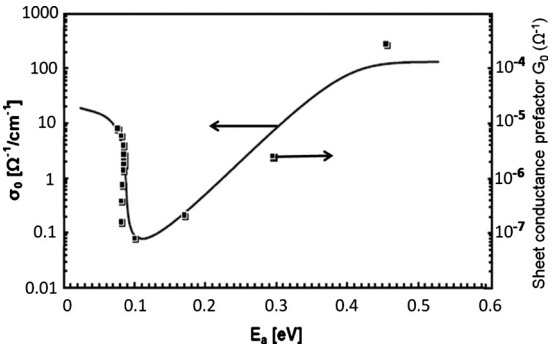


FIG. 8. $\sigma_0$ ($G_0$) as a function of $E_a$ in case of a TFT. Solid line: calculation ($X_c=0.8$, $N_{db}=12.5\times10^{16}$ cm$^{-3}$, $N_d=0$ cm$^{-3}$, $E_c=-0.05$ eV). Squares: data from curve HW-C, Fig. 3 of Meiling e*t al.* (Ref. 28).

transition as a function of $X_c$ our results strongly suggest that $N_d/N_{db}$ in fact increases with $X_c$ (in other words, the dopant concentration increases or the defect concentration decreases) and that the $N_d/N_{db}$ ratio crosses the line $N_d/N_{db}=0.5$ sooner or later.

In Fig. 7 we present for example $\sigma_0$ as a function of $X_c$ were $N_{db}$ and $(1-X_c)N_{db}/N_d$ are kept constant in order to express an increasing dopant density with crystallinity. The value of the latter constant determines where (on the $X_c$ scale) the transition takes place. Here the value is chosen such that the drop in $\sigma_0$ is at an $X_c$ value between 0.75 and 0.8. Let us call this the critical crystallinity $X_s$. The factor by which $\sigma_0$ is decreased at the transition is determined by the absolute values of $N_d$ and $N_{db}$.

A value of about $N_d=10^{16}$ cm$^{-3}$ is representative for these experiments. For $X_c<X_s$ $\sigma_0$ is nearly constant and at $X_c=X_s$ $\sigma_0$ drops by more than two orders of magnitude. For $X_c>X_s$ $\sigma_0$ increases again, presumably because of a fast growing doping/dangling bond ratio. In experiments of Kočka *et al.*[10] and Ram *et al.*[28] $E_a$ is also decreasing for $X_c>X_s$, which leads to the experimentally observed inverse Meyer–Neldel rule (MNR). The lower $E_a$ could be explained by a decrease in the a-Si transport barriers between the nanocrystals. This means that the inverse MNR in this case is a result of two combined effects (the increased doping and the lowering of the transport barriers) and therefore has a totally different origin than the inverse MNR in a TFT.[29]

In TFT's the chemical potential is not changed by doping but can be controlled in a single sample by means of an electrical field. Measurements on $\mu$c-Si layers as the conducting channel between the source and the drain have revealed a normal MNR as well as an inverse MNR behavior.[29] In Fig. 8 we present a calculation of the data for $\sigma_0$ as a function of $E_a$ in the case of a TFT, together with the sheet conductance prefactor ($G_0$) data taken from Meiling and Schropp.[29] The calculation clearly shows both the MNR ($E_{MN}=36$ meV) and the inverse MNR behavior, in accordance with the experiment. The inverse MNR is due to the fact that while $\mu$ approaches the c-Si conduction band, it also enters the tail of a-Si and therefore it effectively changes $\gamma_f$.

In this experiment the critical value for $E_a$ was found to be about 0.1 eV. In order to reproduce this in the calculation we have taken the conduction path 0.1 eV above the c-Si conduction edge. From the calculations we can conclude that the critical value of $E_a$ is a direct measure of the effective height of the barrier between the grains.

In Fig. 9 we have gathered experimental data from the literature in a $\sigma_0$ versus $E_a$ plot and plotted them together with three calculated lines. The effective barrier heights are 0.05 eV, 0.10 eV, and 0.15 eV for, respectively, $E_c=-0.10$ eV, $-0.05$ eV, and 0.00 eV.

The calculated data seem to be covering the experimental data well. For $E_a$ between 0.2 and 0.6 eV (the region where $\mu$ shifts to mid gap) the material obeys the MNR. The corresponding Meyer–Neldel energy from the calculation is found to be 40 meV, which is consistent with values reported from experiments listed by Ram *et al.*[30] The flat region above 0.5 eV in the calculated data is not very recognizable in the experimental data but is in fact found experimentally. The data of Kočka[2] show this most clearly. The reason for this plateau in the calculation of $\sigma_0$ is that $\mu$ is so far away from the conduction band of c-Si that at RT the statistical shift does not occur. The very high values of $\sigma_0$ (>1000 $\Omega^{-1}$ cm$^{-1}$) are found (in Fig. 9) only for the data of Ram *et al.*[28] The reason for this is not known.

It is very remarkable that there is an increase in $\sigma_0$ at low $E_a$ for high $N_d$. Since all experimental points are from different samples it is likely that the samples vary more than

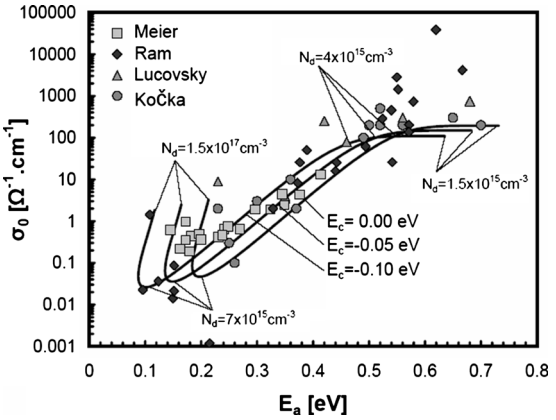


FIG. 9. $\sigma_0$ as a function of $E_a$ and $E_C$. $N_{db}=10^{16}$ cm$^{-3}$ $N_d=0.15-15\times N_{db}$; $E_c=0$, $-0.05$, and $-0.10$ eV. The experimental data is taken from literature Refs. 31, 27, 23, and 2. The parameter that has been varied along each curve is the dopant density ($N_d$). Several values for $N_d$ are indicated along the curves.

one variable ($N_d$,$N_{db}$,$X_c$,$E_c$) from each other. Therefore the points are scattered and are not following one specific curve. However, it seems possible that there are constraints in the relation between $\sigma_0$ and $E_a$ that are not obvious from the model, leading to anti-MNR behavior or an inverse MNR. Ram *et al.*[28] report an anti-MNR for sample with very high crystallinity.

## V. DISCUSSION

The behavior of the activation energy and $\sigma_0$ as a function of crystallinity within the model is in qualitative agreement with experimental observations, like those of Kočka *et al.*[10] and Ram *et al.*,[28] if we assume that the condition $N_d/N_{db}<0.5$ is met for $X_c<X_s$ and $N_d/N_{db}>0.5$ for $X_c>X_s$. From the step in $\sigma_0$ we can estimate the values for $N_d$ and $N_{db}$ near the transition ($N_d/N_{db}=0.5$). For a step from 200 to 1 $\Omega^{-1}$ cm$^{-1}$ $N_d$ is about $2\times10^{16}$ cm$^{-3}$, which is lower than reported oxygen concentrations in some device grade materials.[11] The defect density derived in this way is $10^{16}$ cm$^{-3}$, which is a typical value for spin densities in ESR experiments,[31] but we have to keep in mind that the spread in properties of these materials can be large and it is suggested that high spin densities at high $X_c$ are related to surface effects.[32] Definitive conclusions on this can only be drawn when the conductivity and ESR measurements are done on the very same sample.

In our simulation we did not assume a particular source of doping but oxygen contamination seems to play an important role. Oxygen concentrations of more than $10^{18}$ cm$^{-3}$ are often reported.[33] According to Kamei *et al.*[40] a spin density of $2\times10^{16}$ cm$^{-3}$ corresponds to an oxygen concentration of about $2\times10^{20}$ cm$^{-3}$, which suggests that oxygen incorporation leads predominantly to alloying and doping efficiencies are low, although not negligible. It appears difficult to relate spin density uniquely to an effective doping density, as there are many different ways for oxygen to be incorporated. High concentrations of impurities can accumulate at grain boundaries and can lead to alloying (for example oxides with a wide band gap) and therefore to higher barriers with respect to the a-Si barriers.

Experiments by Kočka *et al.*[10] and Ram *et al.*[28] show that the drop in the activation energy coincides with a morphology change. In our model morphology does not play a role. We are left with four options for the relationship between morphology and change in conduction: (1) it could be coincidence, (2) the morphology change induces a change in sensitivity to doping, (3) the morphology change is caused by the change in doping sensitivity, or (4) the morphology change induces a dramatic change in conduction mechanism as is suggested by Kočka *et al.*[10]

The first option is rather unsatisfactory. The second and third options are hard to decide between. The third option can be motivated by the large change in the chemical potential [see Fig. 2(b)]. A change in $\mu$ can induce a change in reactivity and this may slightly alter the growth mechanism. But the second option seems more likely. The fourth option cannot be ruled out since it is out of the scope of our model.

Regardless of cause and effect, our model is consistent with results from compensation doping experiments. It has been observed that $\sigma_0$ can be lowered over two orders of magnitude and that $E_a$ can be increased by 0.2 eV (Ref. 34) by doping "intrinsic" $\mu$c-Si with boron in order to counterbalance the n-type doping that, for some time, was thought to be unavoidable in the material.[34] The amount of doping at optimal compensation was about 10 ppm of $B_2H_6$ in the gas phase, which translates in 20 ppm of boron doping. We can only guess what the doping efficiency is but 20 ppm is the upper limit of the original n-type doping that was present in the film, which is slightly above the upper range of the values used in Figs. 3 and 4. Kočka *et al.*[10] assume in their model a change in the transport path toward lower energies inside a large grain boundary (LGB) but in our model we do not need to assume such a change in conduction path in order to explain the experimental data.

In our model the lowest possible outcome for $E_a$ is determined by the effective barrier height, which is the distance between the conduction bands of c-Si and a-Si. The lower $E_a$ ($E_a<0.15$ eV) which has been observed experimentally for very high $X_c$,[30] can only be reproduced by the model if we decrease the effective barrier height by lowering the conduction path or changing the band alignment. This change in the a-Si barrier height may happen in reality by a change in band alignment, by accumulation of charged defects at the interfaces, or by thinning of the barrier which enables tunneling.[5] Measurements on TFT's (Refs. 29 and 35) suggest that the effective barrier is indeed lower at high $X_c$.

Conductive atomic force spectroscopy (C-AFM) measurements by Azulay *et al.*[36] seem to suggest that the conduction path is through the amorphous network at high crystallinity ($X_c>0.5$), however, these measurements are influenced by measurement artifacts, as was mentioned by Kocka *et al.*[37]

In contrast with the work of Azulay *et al.*, C-AFM measurements by Mates *et al.*[38] show higher conductivity within the grains, which is more in agreement with our model that predicts a higher electron density in the grains.

From the results of the model calculations we can define different classes of materials: type-1 is a material with a high $E_a$ in which the Fermi level is in the middle of the band and which does not show statistical shift near RT. Most importantly, type-1 has a $\sigma_0$ that is independent of $E_a$. Type-2 is material with the Fermi level between mid gap and the doping level and showing statistical shift at RT. Type-2 obeys the MNR when $X_c$ is changed. Type 3 material has the Fermi level at the doping level and is showing statistical shift at RT. Type 3 has a low activation energy and $\sigma_0$ increases with $X_c$.

The three classes of materials show similar conductivity behaviors as the type-A, type-B, and type-C materials experimentally described by Ram *et al.*,[28] although these authors come up with different conclusions on the origin of the differences in transport properties.

The $E_{MN}$ for type-2 material derived from our simulation corresponds well with that of type-B material. The observed anti-Meyer–Neldel behavior for type-C material, can be explained by our model when a lowering of the barrier height with $X_c$ is included.

Our model is in contrast with the view that the electronic

properties are controlled by percolation.[4] The results by Ram *et al.*[28] already prove that a large change in $E_a$ and $\sigma_0$ can occur without percolation, because their materials are all highly crystalline and still exhibit the anomalous behaviors. In experiments by Kočka *et al.*[10] the critical crystallinity is also much higher than the theoretical percolation threshold of 0.32. In line with our findings, a study of Bronsveld *et al.*[39] does not show any change in electrical behavior at the geometrical percolation threshold. Our EMA predicts threshold behavior for $\sigma_0$ but not for $\sigma$ as a function of $X_c$.

In our model we assume that there is some form of doping which is in principle distributed homogeneously. In Kamei *et al.*,[40] it is found that the impurities are concentrated at grain (agglomerates) boundaries. It is therefore important to investigate how our result would be affected by the doping being concentrated at these boundaries.

We already mentioned that the charge density is in most cases low enough that band bending can be ignored with respect to the small grain sizes. However, if the doping is concentrated at the LGB's, this is not necessarily the case anymore. A consequence would be that the crystalline regions between LGB's will accumulate a net (negative) charge causing some bending of the bands from the center of these crystalline regions to the edges. As a consequence the currents will flow more at the edges of the crystalline regions.

In the LGB region there will be a net (positive) charge but these charges are more localized and will form pits in the potential landscape. We have to keep in mind that at a density of $10^{16}$ $cm^{-3}$ we have only one doping site per crystallite with a diameter of 250 nm, which is about the average size of a large grain.[37] Only at high enough doping density the average barrier height will go down.

A consequence for the simulation would then be that both the a-Si DOS and the $\mu$c-Si DOS are somewhat convoluted in energy space. This, however, would make the inverse MNR transition less steep than seen in the experiment of Meiling and Schropp.[29] In addition, our simulations are able to describe the most important aspects of the behavior of $\sigma_0$ and $E_a$ found in different experiments and by several groups, we think that the concentration of dopants in the boundaries or band bending does not play an important role in the interpretation of the electronic transport behavior.

A deviation of our simulations from experiment (see Fig. 7) does seem to occur at very high $X_c$. This deviation is consistent with lowering of the barrier height (e.g., caused by localization of charges at grain boundaries), or with a higher doping efficiency or higher doping at these high $X_c$ values, both of which are not taken into account in the presented simulations.

## VI. CONCLUSION

We have performed a model calculation of the dc conductivity in microcrystalline material based on an EMA of the DOS. We calculated $E_a$ and $\sigma_0$ as a function of temperature, defect density, doping, and crystallinity. The results are consistent with dc dark conductivity measurements at RT with coplanar contacts and with measurement on TFTs. Our model offers an alternative explanation (in contrast with models assuming a change in conduction path, percolation transport, or a highly conductive amorphous network) for the sharp drop of several orders of magnitude in $\sigma_0$ and the behavior of $E_a$ with increasing crystalline fraction. The sudden drop in $\sigma_0$ with growing $X_c$ or doping is attributed to a transition from a regime with a stationary $\mu$ to a regime with a shifting $\mu$ (statistical shift). The drop in $E_a$ is attributed to enhanced doping efficiency or enhanced doping with growing $X_c$ causing a rise of the Fermi level. Due to the statistical shift $E_a$ decreases even more. The model leads to the same type of distinction into three classes of materials as found in recent literature but based on different principles.


[1] A. L. Baia Neto, A. Lambertz, R. Carius, and F. Finger, J. Non-Cryst. Solids **299–302**, 274 (2002).
[2] J. Kočka, A. Fejfar, H. Stuchliková, J. Stuchlík, P. Fojtík, T. Mates, B. Rezek, K. Luterová, V. Švrček, and I. Pelant, Sol. Energy Mater. Sol. Cells **78**, 493 (2003).
[3] R. Vanderhaghen, S. Kasouit, R. Brenot, V. Chu, J. P. Conde, F. Liu, A. de Martino, P. Roca, and I. Cabarrocas, J. Non-Cryst. Solids **299–302**, 365 (2002).
[4] K. Shimakawa, J. Non-Cryst. Solids **266–269**, 223 (2000).
[5] F. Liu, M. Zhu, Y. Feng, Y. Han, and J. Liu, Thin Solid Films **395**, 97 (2001).
[6] M. Goerlitzer, P. Torres, N. Beck, N. Wyrsch, H. Keppner, J. Pohl, and A. Shah, J. Non-Cryst. Solids **227–230**, 996 (1998).
[7] A. Gordijn, "Microcrystalline silicon for thin-film solar cells," Ph.D. thesis, Utrecht University, 2005.
[8] T. Weis, S. Brehme, P. Kanschat, W. Fuhs, R. Lipperheide, and U. Wille, J. Non-Cryst. Solids **299–302**, 380 (2002).
[9] S. Tripathi, N. Venkataramani, R. O. Dusane, and B. Schroeder, Thin Solid Films **501**, 295 (2006).
[10] J. Kočka, H. Stuchliková, J. Stuchlík, B. Rezek, T. Mates, V. Švrček, P. Foljtík, I. Pelant, and A. Fejfar, J. Non-Cryst. Solids **299–302**, 355 (2002).
[11] S. Vepřek, Z. Iqbal, R. O. Kuhne, P. Capezzuto, F. A. Sarott, and J. K. Gimzewski, J. Phys C, Solid State Phys. **16**, 6241 (1983).
[12] P. Torres, J. Meier, R. Fluckiger, U. Kroll, J. A. Anna Selvan, H. Keppner, A. Shah, S. D. Littelwood, I. E. Kelly, and P. Giannoules, Appl. Phys. Lett. **69**, 1373 (1996).
[13] S. K. Ram, S. Kumar, R. Vanderhaghen, P. Roca, and I. Cabarrocas, J. Non-Cryst. Solids **299–302**, 411 (2002).
[14] N. Wyrsch, C. Droz, L. Feitknecht, P. Torres, E. Vallat-Sauvain, J. Bailat, and A. Shah, J. Non-Cryst. Solids **299–302**, 390 (2002).
[15] R. Biswas and B. C. Pan, NCPV and Solar Program Review Meeting, 2003, Denver, CO, 24–26 March 2003, p. 803.
[16] T. Kamei and T. Wada, J. Appl. Phys. **96**, 2087 (2004).
[17] H. Overhof, M. Otte, M. Schmidtke, U. Backhausen, and R. Carius, J. Non-Cryst. Solids **227–230**, 992 (1998).
[18] N. Wyrsch, P. Torres, M. Goerlitzer, E. Vallat, U. Kroll, A. Shah, A. Poruba, and M. Vanecek, Solid State Phenom. **67–68**, 89 (1999).
[19] H. Overhof and P. Thomas, *Hydrogenated Amorphous Semiconductors* (Springer, Berlin, 1989).
[20] http://www.ioffe.rssi.ru/SVA/NSM/Semicond/Si/bandstr.html
[21] Arizona State University EEE531 Semiconductor Device Theory I.
[22] R. E. I. Schropp and M. Zeman, *Amorphous and Microcrystalline Silicon Solar Cells: Modeling, Materials and Device Technology* (Springer, Boston, 1998).
[23] J. P. Kleider, A. S. Gudovskikh, and P. Roca i Cabarrocas, Appl. Phys. Lett. **92**, 162101 (2008).
[24] C. P. Ewels, "Density functional modeling of point defects in semiconductors," Ph.D. thesis, Exeter University, 1997.
[25] N. F. Mott, Philos. Mag. **26**, 1015 (1972).
[26] G. Lucovsky and H. Overhof, J. Non-Cryst. Solids **164–166**, 973 (1993).
[27] R. A. Street, *Hydrogenated Amorphous Silicon* (Cambridge University Press, Cambridge, UK, 1991).
[28] S. K. Ram, P. Roca i Cabarrocas, and S. Kumar, J. Non-Cryst. Solids **354**, 2263 (2008).
[29] H. Meiling and R. E. I. Schropp, Appl. Phys. Lett. **74**, 1012 (1999).
[30] S. K. Ram, S. Kumar, P. Roca, and I. Cabarrocas, Phys. Rev. B **77**, 045212 (2008).

[31]F. Finger, J. Muller, C. Malten, and H. Wagner, Philos. Mag. B **77**, 805 (1998).
[32]T. Dylla, F. Finger, and R. Carius, *Amorphous and Nanocrystalline Silicon-based Films*, MRS Symposia Proceedings No. 762 (Materials Research Society, Pittsburgh, 2003), p. A2.5.
[33]T. Kamei and A. Matsudo, *Amorphous Silicon Technology*, MRS Symposia Proceedings No. 557 (Materials Research Society, Pittsburgh, 1999), p. 19.
[34]J. Meier, S. Dubail, R. Fluckiger, D. Fischer, H. Keppner, and A. Shah, Proceedings of the 1994 IEEE First World Conference on Photovoltaic Energy Conversion, Waikoloa, Hawaii, December 5–9, 1994 (IEEE, New York, 1994), Vol. 1, pp. 409–412.
[35]J. Puigdollers, C. Voz, A. Orpell, I. Martin, D. Soler, M. Fonrodona, J. Beromeu, J. Andrea, and R. Alcubilla, J. Non-Cryst. Solids **299–302**, 400 (2002).
[36]D. Azulay, I. Balberg, V. Chu, J. P. Conde, and O. Millo, Phys. Rev. B **71**, 113304 (2005).
[37]J. Kočka, A. Vetushka, and A. Fejfar, Philos. Mag. **89**, 2557 (2009).
[38]T. Mates, P. C. P. Bronsveld, A. Fejfar, B. Rezek, J. Kočka, J. K. Rath, and R. E. I. Schropp, J. Non-Cryst. Solids **352**, 1011 (2006).
[39]P. C. P. Bronsveld, A. Verkerk, T. Mates, A. Fejfar, J. K. Rath, and R. E. I. Schropp, *Amorphous and Polycrystalline Thin-Film Silicon Science and Technology*, MRS Symposia Proceedings No. 989 (Materials Research Society, Pittsburgh, 2007), p. 159.
[40]T. Kamei, T. Wada, and A. Matsuda, *Amorphous and Heterogeneous Silicon-Based Films*, MRS Symposia Proceedings No. 664 (Materials Research Society, Pittsburgh, 2001), p. A.10.1.1-6.